

Gravitational Waves from Resonant Transitions of Tidally Perturbed Gravitational Atoms

Antonios Kyriazis,¹ Fengwei Yang²

¹*Department of Physics, University of Florida, Gainesville, FL 32611, U.S.A.*

²*Institute for Fundamental Theory, Department of Physics, University of Florida, Gainesville, FL 32611, U.S.A.*

E-mail: akyriazis@ufl.edu, fengwei.yang@ufl.edu

ABSTRACT: Light bosons can form a gravitational atom (GA) around a spinning black hole through the superradiance process. Considering the black hole to be part of a binary system, the tidal potential of the companion periodically perturbs the GA such that an “atomic” transition occurs between two of its energy eigenstates. The resonant transition is modeled by the Landau-Zener system, where the orbital frequency of the companion determines the relevant transition. In this work, we study a novel gravitational wave signal originating directly from the *atomic transition* of the GA in a *binary* system. We derive the analytical formulae of both the strain waveform and frequency spectrum of the signal. We further present the GA-binary systems that can have a large signal-to-noise ratio in LISA’s frequency band. Finally, we discuss the implications of detection of the signal: inferring model parameters, including the boson mass and black hole spin, and computing the phase shift and Doppler shift of the gravitational wave signal for equal mass binaries.

Contents

1	Introduction	1
2	Gravitational Atoms in isolation and in binaries	3
2.1	The Gravitational Atom	3
2.2	The perturbed Gravitational Atom	4
2.3	The adiabaticity parameter	7
2.4	The decay rate of the final state	8
3	Gravitational waves from transitions	10
3.1	The quadrupole approximation	10
3.2	The frequency spectrum	14
3.3	The signal-to-noise ratio	17
4	Implications	19
4.1	LISA binary systems	19
4.2	Breaking degeneracies by spectral information	20
4.3	Dependence on mass ratio q : phase shift and Doppler shift	21
5	Conclusion	22
A	Gravitational atom basics	24
A.1	Tidal field of the companion	24
A.2	Dressed frame Hamiltonian	25
B	Axially asymmetric density from interference	25
C	The mass of the GA	27

1 Introduction

In black hole physics, superradiance is a process that can extract mass and angular momentum from a spinning black hole. It is triggered when a wave that scatters by the black hole satisfies the condition [1]:

$$\omega < m\Omega_H, \tag{1.1}$$

where ω is the frequency of the wave, Ω_H is the angular velocity of the black hole and m is the azimuthal number with respect to the rotation axis. In addition, if the bosonic particles that make up the wave have a small mass, such as axions or axion-like particles [2, 3], they can form hydrogen-like bound states around the black hole, hence the term

“gravitational atom” (GA) [4, 5]. Using the measurements of black holes’ spins in X-ray binaries, constraints have been placed on these light particles [6–13].

The bosons of this GA can annihilate to produce gravitational wave signals with frequency 2μ , where μ is the boson’s mass, or spontaneously transition between two superradiant states, again producing a gravitational wave signal with frequency equal to the energy difference between the states. These types of signals can be searched for in LIGO and LISA [6, 14, 15]. The inclusion of self-interactions induces mixing between superradiant states that leads to a gravitational wave signal in the deci-Hz frequency range and can also be searched for in ground-based interferometers [12, 16, 17].

The GA presents rich and intriguing phenomena when perturbed via a companion compact object [18]. The tidal field of the companion induces resonant transitions between the growing and decaying states of the cloud, causing its demise. The question is: are there any observable signals from these transitions? By using conservation of angular momentum, it has been shown that a transition can back-react to the orbit, causing the orbital frequency to either “float” or “sink”, depending on the type of transition. This can leave distinct imprints on the binary’s waveform, a smoking gun signature for the presence of a GA [19–27]. Another distinct effect of the back-reaction is the increase of the orbit’s eccentricity, while the orbit is within the resonance band. This will drastically alter the distribution of black hole masses and eccentricities in black hole binary systems that are expected to be observed by LISA [28]. Off-resonant mixing between growing and decaying states may also prevent superradiance all together or cause the decay of the GA, if it has grown, while the back-reaction can, also in this case, leave observable imprints on the inspiral’s waveform [29].

Whereas most of the literature on this topic has focused on the effects that the GA may have on the gravitational wave signal of the binary, in this paper we point out a *novel* gravitational wave signal that comes from the GA itself, ignoring the back-reaction to the orbit. It was discussed in [20] that during the transition of the GA from one state to another, it obtains a time-dependent quadrupole moment, due to the interference of the two states. Starting from this observation, we calculate the second time derivatives of these quadrupole moments and derive expressions for the strains of the gravitational waves that are produced during the transition. These gravitational waves originate from the GA and they would be a direct probe of its properties, if detected.

We find that the features of this new gravitational wave signal, such as the duration, strength, peak frequency, and frequency spread can be derived from first principles and depend on the parameters of the binary system and the boson mass. Our main focus is on hyperfine and fine transitions (as defined in [18]). The advantage is that these take place when the companion is still far away from the cloud, allowing a perturbative treatment of the tidal field. In essence, the quadrupole moment of the tidal field dominates and we can neglect higher multipoles. If the orbit is quasicircular and on the equatorial plane of the GA, the selection rules allow only for a handful of transitions to take place. In the formalism that we develop, we also take into account the decay rate of the final state into the black hole, which can significantly alter the transition’s properties [27].

The frequency of these types of events can be in LISA’s frequency band and so we scan

the parameter space of black hole masses, mass ratios of companions, and boson masses to determine which type of systems give the most promising signal-to-noise ratio (SNR). We also delve into which parameters of the system one could determine if such a gravitational wave were indeed detected, and estimate the phase shift of the signal due to the motion of the rotating black hole around the center of mass of the binary.

The paper is structured as follows: in section 2, we review in brief some basic properties of the GA, the Landau-Zener transition of a two-state system, and the effects of including the decay rate of the second mode. In section 3, we present the formalism for the computation of the gravitational wave strain waveform and frequency spectrum produced during a given transition. In section 4, we discuss the implications of detection of the gravitational wave signal from a GA-binary system. We conclude in section 5 with some remarks on the prospects for future investigations in this topic.

2 Gravitational Atoms in isolation and in binaries

2.1 The Gravitational Atom

In this section, we give a brief overview of the GA, establishing also the conventions we will be using throughout. An important quantity is the “fine-structure” constant of a GA, defined as the ratio of the gravitational radius of the black hole to the Compton wavelength of the boson:

$$\alpha \equiv \frac{r_g}{\lambda_c} = \mu M, \quad (2.1)$$

where we use the Planck unit throughout the paper, $G = c = \hbar = 1$. In the case where the particle is non-relativistic we can approximate $\omega \approx \mu$. The angular velocity of the Kerr black hole is given by $\Omega_H = \frac{\tilde{a}}{2r_+}$, where $\tilde{a} = \frac{a}{M} \leq 1$ is its dimensionless spin and $r_+ = M + \sqrt{M^2 - a^2}$ is its outer horizon [30]. The condition of superradiance eq. (1.1) can be re-expressed as an inequality for α :

$$\alpha < \frac{m}{2} \frac{\tilde{a}}{1 + \sqrt{1 - \tilde{a}^2}}. \quad (2.2)$$

Thus, eq. (2.2) determines the upper bound of the fine-structure constant α given the spin of the black hole \tilde{a} and the azimuthal quantum number m of the GA. For maximally spinning black holes, $\tilde{a} = 1$, the $m = 1$ states can only grow for $\alpha < 0.5$. If the black hole starts off with $\tilde{a} \ll 1$, the upper bound of α becomes more stringent, but for simplicity, we assume throughout an initially maximally spinning black hole. The saturated spin of the black hole can be obtained by rearranging eq. (2.2),

$$\tilde{a}_{\text{crit}} = \frac{4m\alpha}{m^2 + 4\alpha^2}. \quad (2.3)$$

The equation of motion of the non-relativistic scalar field produced by superradiance is described by a Schrödinger-like equation in the limit $r \gg M$ and $\alpha \ll 1$ [4]:

$$i\partial_t\psi(t, \vec{x}) = \left(-\frac{\nabla^2}{2\mu} - \frac{\alpha}{r} \right) \psi(t, \vec{x}). \quad (2.4)$$

The size of the cloud is characterized by its Bohr radius $r_c = \frac{M}{\alpha^2}$. The bound states are given by:

$$\psi_{nlm}(t, \vec{x}) = e^{-i(\omega_{nlm} - \mu)t} R_{nl}(r) Y_{lm}(\theta, \varphi), \quad (2.5)$$

where n, l, m are the principal, angular, and azimuthal quantum numbers respectively, ω_{nlm} is the eigenfrequency of the eigenstate $|nlm\rangle$, which is generally complex due to the purely incoming boundary conditions at the black hole's outer horizon, $R_{nl}(r)$ is the hydrogenic radial wavefunction, and $Y_{lm}(\theta, \varphi)$ are the spherical harmonics. This non-relativistic approach holds very well if $\alpha \lesssim 0.2$, while it starts to break down for larger values of α and numerical approaches are required to solve the equation of motion [5].

The real part of the eigenfrequencies gives the energy levels of the gravitational atom, while the imaginary part gives the instability rates [4–6]:

$$\omega_{R,nlm} = \mu \left(1 - \frac{\alpha^2}{2n^2} - \frac{\alpha^4}{8n^4} + \left(\frac{2}{n} - \frac{6}{2l+1} \right) \frac{\alpha^4}{n^3} + \frac{16\tilde{a}m\alpha^5}{n^3 2l(2l+1)(2l+2)} + \mathcal{O}(\alpha^6) \right), \quad (2.6)$$

$$\Gamma_{nlm} \equiv \omega_{I,nlm} = \frac{2r_+}{M} C_{nlm}(\alpha, \tilde{a})(m\Omega_H - \mu)\alpha^{4l+5}, \quad (2.7)$$

where C_{nlm} are coefficients that can be readily found in [5]. Notice how in eq. (2.6) the first two terms are the same as with the regular hydrogen atom. The fourth term is what will be relevant for the so-called fine transitions ($\Delta n = 0, \Delta l \neq 0$) while the fifth term, in which the black hole's spin breaks the degeneracy of the third quantum numbers, is relevant for the hyperfine transitions ($\Delta n = 0, \Delta l = 0, \Delta m \neq 0$). Since we are in the limit $\alpha \ll 1$, eq. (2.7) implies that the fastest growing superradiant levels are those with $l = m$, with the $l = m = 1$ being the fastest. An estimate for the growth timescale of the fastest growing mode, around a maximally spinning black hole, is

$$\Gamma_{211}^{-1} \approx 247 \text{ days} \left(\frac{M}{10^4 M_\odot} \right) \left(\frac{0.2}{\alpha} \right)^9 \left(\frac{0.6}{1-2\alpha} \right)^3. \quad (2.8)$$

2.2 The perturbed Gravitational Atom

In this section, we start to consider the GA in a binary system setup and summarize the results from the literature that are relevant to the later analysis. The companion induces a tidal field $V_*(t, \vec{r})$ on the GA that will cause it to undergo transitions between states. We will assume that the companion is far away so that we can treat the tidal field perturbatively. The exact form of the mixing between the states is given in several works [18, 20, 22] and is also given for reference in appendix A.1. For our purposes, it is important to note that if the companion is far from the GA, the dominant multipole moment of the tidal field is the *quadrupole* moment, $l_* = 2$. This leads to mixing between two states and the following selection rules are derived:

$$m_f - m_i = m_*, \quad (2.9)$$

$$|l_i - l_f| \leq 2 \leq l_i + l_f, \quad (2.10)$$

$$l_i + l_f = 2p - 2, p \in \mathbb{Z}, \quad (2.11)$$

where i, f represent the initial and final states respectively and m_* is the azimuthal number of the spherical harmonics of the tidal field quadrupole. Throughout the paper, we make the following two assumptions:

- The orbit is quasi-circular.
- The companion is on the same equatorial plane as the cloud.

With these assumptions, only states that satisfy $m_* = \pm 2 = m_f - m_i$ couple to each other as demanded by the selection rule, and the mixing between two different states takes a simple form:

$$\langle \psi_f | V_*(t, \vec{r}) | \psi_i \rangle = \eta e^{-im_*\varphi_*}, \quad (2.12)$$

where η denotes the amplitude of the mixing with its explicit expression given in eq. (A.6) and φ_* is the phase of the binary, whose derivative is the frequency of the orbit, $\dot{\varphi}_*(t) = \pm\Omega(t)$ [18, 20]. The plus (minus) sign is for co(counter)-rotating orbits. The matrix element in eq. (2.12) is akin to a periodic, external driving force, and a resonance is expected to take place when the frequency of this force is equal to the energy splitting of the two states $|m_*|\Omega = \Delta\omega_R \equiv \omega_{R,i} - \omega_{R,f}$.

The orbit of the companion evolves very slowly during the transition¹ due to the emission of gravitational waves, so that the frequency can be linearized as a function of time t [20]:

$$\Omega(t) \approx \Omega_0 + \gamma t, \quad (2.13)$$

where Ω_0 is the reference frequency at $t = 0$ and γ is the change rate of the orbital frequency due to gravitational wave emission,

$$\frac{\gamma}{\Omega_0^2} = \frac{96}{5} \frac{q}{(q+1)^{1/3}} (M\Omega_0)^{5/3}, \quad (2.14)$$

where q is the ratio of the companion mass to the central black hole mass M . The linear approximation of the orbital frequency is valid for the time within $-\Omega_0/\gamma \lesssim t \lesssim \Omega_0/\gamma$. The Hamiltonian that governs the evolution of the coefficients of the initial and final states of a two-state system, $c_i(t)$ and $c_f(t)$, that are mixed via the perturbing potential eq. (A.6), is given by :

$$\mathcal{H} = \begin{pmatrix} -\Delta\omega_R/2 & \eta e^{i\Delta m\varphi_*(t)} \\ \eta e^{-i\Delta m\varphi_*(t)} & \Delta\omega_R/2 - i|\Gamma| \end{pmatrix}, \quad (2.15)$$

where $\Delta\omega_R = \omega_f - \omega_i$, $\Delta m = m_f - m_i$, and Γ is the instability rate of the final state (see eq. (2.7)), which is a decaying mode considered here. By performing a unitary transformation of \mathcal{H} to the co-rotating (or dressed) frame, one can eliminate the fast oscillations of

¹Back-reaction effects affect the transition in two ways: 1. they shift the resonance frequency of the LZ transition; 2. they vary the change rate of the orbital frequency. For the 211 hyperfine transition we considered throughout the paper, we checked the resonance frequency is only shifted by $\mathcal{O}(1\%)$ [22] and the variation of the orbital frequency due to the angular momentum transfer from the cloud to the binary orbit is only relevant over a short time scale near the resonance, and hence we neglect it here.

the off-diagonal elements, and the coefficients transform accordingly

$$\begin{pmatrix} c_i(t) \\ c_f(t) \end{pmatrix} = \begin{pmatrix} e^{i\Delta m\varphi_*(t)/2} & 0 \\ 0 & e^{-i\Delta m\varphi_*(t)/2} \end{pmatrix} \begin{pmatrix} d_i(t) \\ d_f(t) \end{pmatrix}. \quad (2.16)$$

Since it has been used widely in the literature, we only provide the Hamiltonian in this dressed frame in appendix A.2. When setting the reference orbital frequency to match the energy splitting of the transition $\Omega_0 = \pm \frac{\Delta\omega_R}{\Delta m}$ and applying the linear orbital frequency approximation, in eq. (2.13), the Hamiltonian \mathcal{H} is reduced to the well known Landau-Zener system [31, 32]. The main point is that a transition will take place at frequency Ω_0 . In this paper, we will primarily deal with hyperfine and fine transitions, whose orbital frequency can be found from eq. (2.6),

$$\Omega_{0,\text{hyp}} = \frac{64m_i\alpha^7}{Mn^3 2l(2l+1)(2l+2)(m_i^2 + 4\alpha^2)}, \quad (2.17)$$

$$\Omega_{0,\text{fine}} = \frac{\Delta l}{\Delta m} \frac{12\alpha^5}{Mn^3(2l_i+1)(2l_f+1)}. \quad (2.18)$$

where we assumed for hyperfine transitions that the black hole's spin is given by eq. (2.3), and the subscript of l and m represents the associated initial or final state. An advantage of working with hyperfine and fine transitions is that they take place when the companion is far away from the GA, and so keeping only the quadrupole term in the tidal field is justified [33]. We will consider hyperfine transitions from the 211 state and fine transitions from the 322 state. The selection rules that we discussed above demand $211 \rightarrow 21-1$ and $322 \rightarrow 300$. Since $\Delta m = -2$ and $\Delta E < 0$, only co-rotating orbits can induce these transitions, which we will consider throughout the paper.

In addition, the frequency of these transitions happens to fall in LISA's band. For example, we have for the $211 \rightarrow 21-1$ transition:

$$f_{0,211} \approx 1\text{mHz} \left(\frac{\alpha}{0.4}\right)^7 \left(\frac{10^4 M_\odot}{M}\right) \left(\frac{1.64}{1+4\alpha^2}\right). \quad (2.19)$$

Similarly, for the fine transition we are considering, we have

$$f_{0,322} \approx 5.6\text{mHz} \left(\frac{\alpha}{0.5}\right)^5 \left(\frac{10^5 M_\odot}{M}\right). \quad (2.20)$$

An important parameter that characterizes the transition is the *adiabaticity* parameter:

$$z \equiv \frac{\eta^2}{|\Delta m|\gamma}. \quad (2.21)$$

The remaining population of the first state long after the transition is given by $|d_1(t \rightarrow \infty)|^2 = e^{-2\pi z}$. If the adiabaticity $z \gg 1$, the transition is adiabatic: the two states exchange populations. When $z \lesssim 1$, the transition is non-adiabatic and only a fraction of the bosons is transferred. We demonstrate the evolution of the states in these two cases in fig. 1.

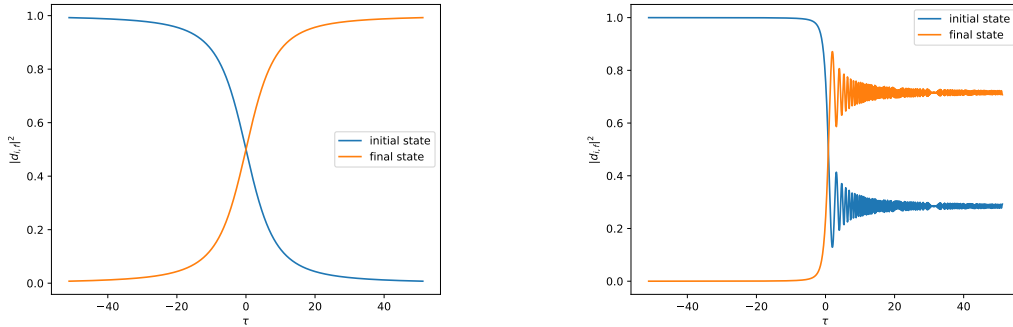


Figure 1: The adiabatic and non-adiabatic transitions for $z = 20$ (left) and $z = 0.2$ (right).

In the co-rotating frame, the Hamiltonian is transformed to a simpler form $\bar{\mathcal{H}}$ (see eq. (A.8)) and the coefficients d_1 and d_2 evolve according to

$$i \frac{dd_a}{dt} = \sum_b \bar{\mathcal{H}}_{ab}(t) d_b, \quad a, b = 1, 2. \quad (2.22)$$

The solutions with the initial conditions $|d_1(t \rightarrow -\infty)|^2 = 1$ and $|d_2(t \rightarrow -\infty)|^2 = 0$ have an analytical form in terms of the parabolic cylinder function [34],

$$d_1(t) = e^{-\frac{\pi z}{4}} D_{iz}(e^{\frac{3i\pi}{4}} \sqrt{|\Delta m|} \gamma t), \quad (2.23)$$

$$d_2(t) = \sqrt{z} e^{-\frac{\pi z}{4}} D_{iz-1}(e^{\frac{3i\pi}{4}} \sqrt{|\Delta m|} \gamma t). \quad (2.24)$$

2.3 The adiabaticity parameter

The parameter z is important in the analysis of the Landau-Zener system, and so in this subsection we will determine its scaling in terms of α and q for the transitions of interest.

To begin, if the distance of the companion is much larger than the size of the cloud, we may ignore the second term in eq. (A.6). In general, the ratio between the companion distance and the cloud size is given by

$$\frac{R_*}{r_c} = \frac{(1+q)^{1/3} \alpha^2}{(M\Omega)^{2/3}}. \quad (2.25)$$

Substituting the $|211\rangle$ hyperfine transition and $|322\rangle$ fine transition frequencies, we get explicitly

$$\frac{R_{211 \rightarrow 21-1}}{r_c} \approx 33 \left(\frac{1+4\alpha^2}{1.81} \right)^{2/3} \left(\frac{1+q}{1.1} \right)^{1/3} \left(\frac{0.45}{\alpha} \right)^{8/3}, \quad (2.26)$$

$$\frac{R_{322 \rightarrow 300}}{r_c} \approx 18 \left(\frac{1+q}{1.1} \right)^{1/3} \left(\frac{0.45}{\alpha} \right)^{4/3}. \quad (2.27)$$

This approximation works best for small values of α , while it is not particularly sensitive to the mass ratio. Having justified it for the transitions of interests, we neglect the I_{out}

integral in eq. (A.6) and obtain the following expression for the adiabaticity parameter of the 211 \rightarrow 21-1 transition:

$$z_{211 \rightarrow 21-1} \approx 7 \left(\frac{1.81}{1+4\alpha^2} \right)^{1/3} \left(\frac{q}{1} \right) \left(\frac{2}{1+q} \right)^{5/3} \left(\frac{0.45}{\alpha} \right)^{11/3}. \quad (2.28)$$

For the benchmark value of α , the 211 transition will become non-adiabatic for mass ratios $q \lesssim 0.049$. Therefore, this parameter is $\mathcal{O}(1)$ for equal mass binaries, while it is much smaller than one for intermediate and extreme mass ratio inspirals. For the 322 \rightarrow 300 transition, we find

$$z_{322 \rightarrow 300} \approx 140 \left(\frac{q}{1} \right) \left(\frac{2}{1+q} \right)^{5/3} \left(\frac{0.45}{\alpha} \right)^{13/3}, \quad (2.29)$$

so it will be larger than the 211 \rightarrow 21-1 for the same values of α and q .

2.4 The decay rate of the final state

So far, we have ignored the decay of the final state into the black hole. However, if the mixing between the states is subdominant compared to the decay rate Γ , i.e. $\eta \ll |\Gamma|$, the evolution of the coefficients d_1 and d_2 will be significantly different from what we laid out above. In eqs. (2.30) and (2.31) we evaluate the ratio of the mixing strength η with the decay rate $|\Gamma|$. The latter is calculated assuming that the black hole is at the saturated spin of the corresponding initial state and we may approximate it as $|\Gamma_{21-1}| \approx \alpha^{10}/(6M)$ and $|\Gamma_{300}| \approx 8\alpha^6/(27M)$, where we have used the analytical expressions that can be found in [4–6] in the limit $\alpha \ll 1$. The relevant ratios are

$$\frac{\eta_{211 \rightarrow 21-1}}{|\Gamma_{21-1}|} \approx 7.5 \times 10^{-2} \left(\frac{q}{0.1} \right) \left(\frac{1.1}{1+q} \right) \left(\frac{\alpha}{0.45} \right) \left(\frac{1.81}{1+4\alpha^2} \right)^2, \quad (2.30)$$

$$\frac{\eta_{322 \rightarrow 300}}{|\Gamma_{300}|} \approx 3 \times 10^{-2} \left(\frac{q}{0.1} \right) \left(\frac{1.1}{1+q} \right) \left(\frac{\alpha}{0.45} \right), \quad (2.31)$$

and therefore, the decay of the second mode needs to be taken into account for a wide range of parameters. There are analytical results for the coefficients d_1 and d_2 in terms of the parabolic cylinder functions that can be readily used [35, 36]:

$$d_1(t) = e^{-\frac{|\Gamma|t}{2} - \frac{\pi z}{4}} D_{iz} \left(e^{\frac{3i\pi}{4}} \left(\sqrt{\gamma|\Delta m|}t - i \frac{|\Gamma|}{\sqrt{\gamma|\Delta m|}} \right) \right), \quad (2.32)$$

$$d_2(t) = e^{-\frac{|\Gamma|t}{2} - \frac{\pi z}{4}} \sqrt{z} D_{iz-1} \left(e^{\frac{3i\pi}{4}} \left(\sqrt{\gamma|\Delta m|}t - i \frac{|\Gamma|}{\sqrt{\gamma|\Delta m|}} \right) \right). \quad (2.33)$$

Specializing to the case where $\eta \ll \Gamma$, we can simplify these to [27]:

$$|d_1(t)|^2 = \exp \left[-z \left(\pi + 2 \tan^{-1} \left(\frac{|\Delta m| \gamma t}{|\Gamma|} \right) \right) \right], \quad (2.34)$$

$$d_2(t) = -\frac{i\eta}{i|\Delta m| \gamma t + |\Gamma|} d_1(t). \quad (2.35)$$

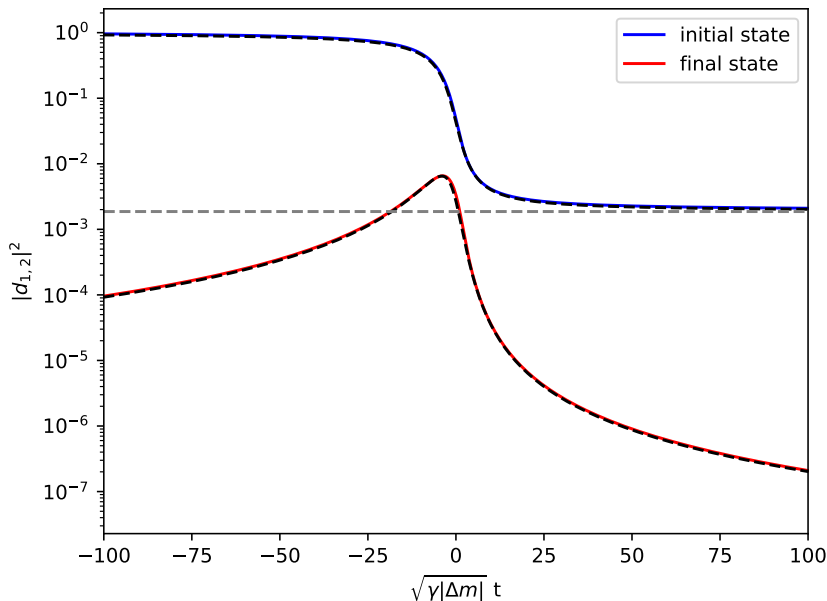


Figure 2: Comparison of the numerical solution of eq. (A.8) and the analytical results in eq. (2.34). We have chosen $z = 1$ and $\frac{\eta}{|\Gamma|} = 0.25$. Solid lines are the numerical results and black dashed lines are the analytical approximation. The horizontal grey dashed line is the asymptotic value $e^{-2\pi z}$.

The perturbation starts to act roughly at time $t_I \sim -\frac{\Gamma}{2\gamma}(1+2z)$ [27]. In the limit $|d_1(t \rightarrow \infty)|^2 \rightarrow e^{-2\pi z}$, we recover the same result as in the Landau-Zener system for the initial state. In the $t \rightarrow \pm\infty$ limit, the occupation number of the second state is zero, while at $t = 0$ it is suppressed by the factor $\frac{\eta}{|\Gamma|}$, a reflection of the fast decay rate of the bosons. In fig. 2, we plot the numerical and the analytical solutions eqs. (2.34) and (2.35) for a certain choice of the ratio $\frac{\eta}{|\Gamma|}$. The agreement is very good between the two.

One issue that needs to be addressed is whether the initial time t_I is earlier than the time when the binary enters the resonant band. If that is the case, the linear approximation that we employed in eq. (2.13) no longer holds and we would have to take into account the non-linear evolution of the binary. The condition for the approximation to break down is:

$$\frac{\gamma|t_I|}{\Omega_0} \approx \frac{|\Gamma|(1+2z)}{2\Omega_0} \sim \mathcal{O}(1). \quad (2.36)$$

In fig. 3, we plot the contours in an $\alpha - q$ plane where eq. (2.36) is satisfied for the transitions we are studying. For the $211 \rightarrow 21-1$ transition, this is an issue for equal mass binaries, where $z \sim \mathcal{O}(1)$. The fine transition $322 \rightarrow 300$ covers a large parameter space because the 300 state has a very large decay rate. The parameter space for this transition shrinks further when the effect of the termination of superradiance due to the off-resonant mixing of the two states is considered, which excludes mass ratios that satisfy $q \gtrsim 10^{-4}$ (this affects all fine transitions while the $211 \rightarrow 21-1$ is unaffected) [29]. In light of these observations, we will only consider the $211 \rightarrow 21-1$ transition for the rest of the paper in

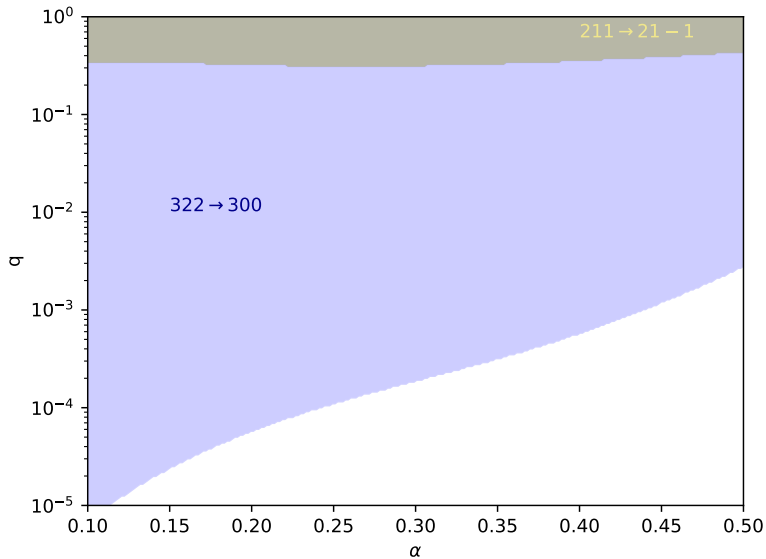


Figure 3: Regions in the $\alpha - q$ plane where the linear approximation of the orbital evolution is invalid for the $|211\rangle$ hyperfine transition and $|322\rangle$ fine transition.

the appropriate parameter space and we will consider a more complete treatment of the $322 \rightarrow 300$ in the future.

3 Gravitational waves from transitions

3.1 The quadrupole approximation

In this section, we present the formalism that we developed to calculate the gravitational waves that are emitted from the GA while the transition is taking place. The state of the GA is a superposition of the two states that participate in the transition

$$\psi(t, \vec{x}) = \sqrt{N} (c_1(t)\psi_1(\vec{x}) + c_2(t)\psi_2(\vec{x})), \quad (3.1)$$

where N is the number of axions. The density is given by:

$$\rho(t, \vec{x}) = \mu |\psi(t, \vec{x})|^2 = M_c (|c_1(t)|^2 |\psi_1|^2 + |c_2(t)|^2 |\psi_2|^2 + 2\Re(c_1^*(t)c_2(t)\psi_1^*\psi_2)), \quad (3.2)$$

where $M_c = \mu N$ is the mass of the cloud. We stress that the usual normalization condition $|c_1(t)|^2 + |c_2(t)|^2 = 1$ does not apply here because of the decay rate of the second state, which loses axions to the black hole. We can calculate the mass quadrupoles:

$$M_{ij} = \int d^3x \rho(t, \vec{x}) x_i x_j, \quad (3.3)$$

for a given pair of states ψ_1 and ψ_2 and their second-order time derivatives will give us the strain of the gravitational waves emitted during the transition. The quadrupole approximation holds in general if the wavelength of the emitted gravitational waves is much

larger than the size of the source [37]. We will justify that it works once we calculate the frequency of the signal in the next subsection.

For the hyperfine $211 \rightarrow 21-1$ transition, using the wavefunctions of the hydrogen atom [38], we obtain:

$$M_{11}(t) = 12M_c r_c^2 \left(1 - \Re \left[d_1^*(t_{\text{re}}) d_2(t_{\text{re}}) e^{-2i\Delta m \varphi(t_{\text{re}})} \right] \right), \quad (3.4)$$

$$M_{22}(t) = 12M_c r_c^2 \left(1 + \Re \left[d_1^*(t_{\text{re}}) d_2(t_{\text{re}}) e^{-2i\Delta m \varphi(t_{\text{re}})} \right] \right), \quad (3.5)$$

$$M_{12}(t) = -12M_c r_c^2 \Im \left[d_1^*(t_{\text{re}}) d_2(t_{\text{re}}) e^{-2i\Delta m \varphi(t_{\text{re}})} \right], \quad (3.6)$$

$$M_{33}(t) = 6M_c r_c^2 (|d_1(t_{\text{re}})|^2 + |d_2(t_{\text{re}})|^2), \quad (3.7)$$

where we used the unitary matrix from eq. (2.16) to express the coefficients in the co-rotating frame and defined the retarded time $t_{\text{re}} \equiv t - r$, with r the distance between the GA and the observer. The M_{13} and M_{23} coefficients are zero due to the integral over the azimuthal angle. In appendix B, we explain in more detail how the interference of the two states gives rise to an axially asymmetric mass density.

The second time derivatives of the above mass quadrupole moments will determine the gravitational wave strain from the transition, which eventually are dependent on the second time derivatives of d_1 and d_2 . The equations of motion for d_1 and d_2 in eq. (2.22) can be used to re-express their second time derivatives in terms of the known solutions d_1 and d_2 . However, the leading order term of \ddot{M}_{ij} , $i, j = 1, 2, 3$, can be obtained in the following way easier: in the $\eta \ll |\Gamma|$ limit, when a time derivative acts on $d_{1,2}$ given by eq. (2.34) and eq. (2.35), the result is of order $\mathcal{O}\left(\frac{\gamma}{|\Gamma|} d_{1,2}\right)$. When the time derivative acts on the exponential function $e^{-2i\Delta m \varphi(t_{\text{re}})}$, it brings down a factor of $\Omega \sim \Omega_0$. By factoring out Ω_0^2 , the remaining terms are of order $\mathcal{O}\left(\frac{\gamma^2}{\Omega_0^2 |\Gamma|^2}, \frac{\gamma}{\Omega_0 |\Gamma|}\right)$, which scale like $\mathcal{O}(\alpha^{52/3}, \alpha^{26/3})$ for the $211 \rightarrow 21-1$ transition, so they can be ignored. Keeping only the leading order term, the final result is

$$\ddot{M}_{11}(t) = -\ddot{M}_{22}(t) = 12M_c r_c^2 \Omega_0^2 \Re \left[e^{-2i\Delta m \varphi(t_{\text{re}})} Q(t_{\text{re}}) \right], \quad (3.8)$$

$$\ddot{M}_{12}(t) = 12M_c r_c^2 \Omega_0^2 \Im \left[e^{-2i\Delta m \varphi(t_{\text{re}})} Q(t_{\text{re}}) \right], \quad (3.9)$$

$$Q(t) \approx 4|\Delta m|^2 d_1^*(t_{\text{re}}) d_2(t_{\text{re}}) + \mathcal{O}\left(\frac{\gamma}{\Omega_0 |\Gamma|}\right), \quad (3.10)$$

where we have ignored \ddot{M}_{33} because it is suppressed by $\mathcal{O}\left(\frac{\gamma^2}{\Omega_0^2 |\Gamma|^2}\right)$ relative to the other components. The factor Q can be found from eq. (2.34) and eq. (2.35) in the limit where $\eta \ll |\Gamma|$. The latter case is easier to handle analytically and it is straightforward to find that the maximum value of $|Q|$ occurs at $t_{\text{max}} = -\frac{2z|\Gamma|}{|\Delta m|\gamma} = -\frac{z|\Gamma|}{\gamma}$. This result persists for the more general formula as long as $\eta \lesssim |\Gamma|$.

The strain of the plus- and cross-polarized gravitational wave is given by [37],

$$h_{+,211}(t) = h_0 \frac{1 + \cos^2(\iota)}{2} \Re \left[e^{-2i\Delta m \varphi(t_{\text{re}})} Q(t_{\text{re}}) \right], \quad (3.11)$$

$$h_{\times,211}(t) = h_0 \cos(\iota) \Im \left[e^{-2i\Delta m \varphi(t_{\text{re}})} Q(t_{\text{re}}) \right], \quad (3.12)$$

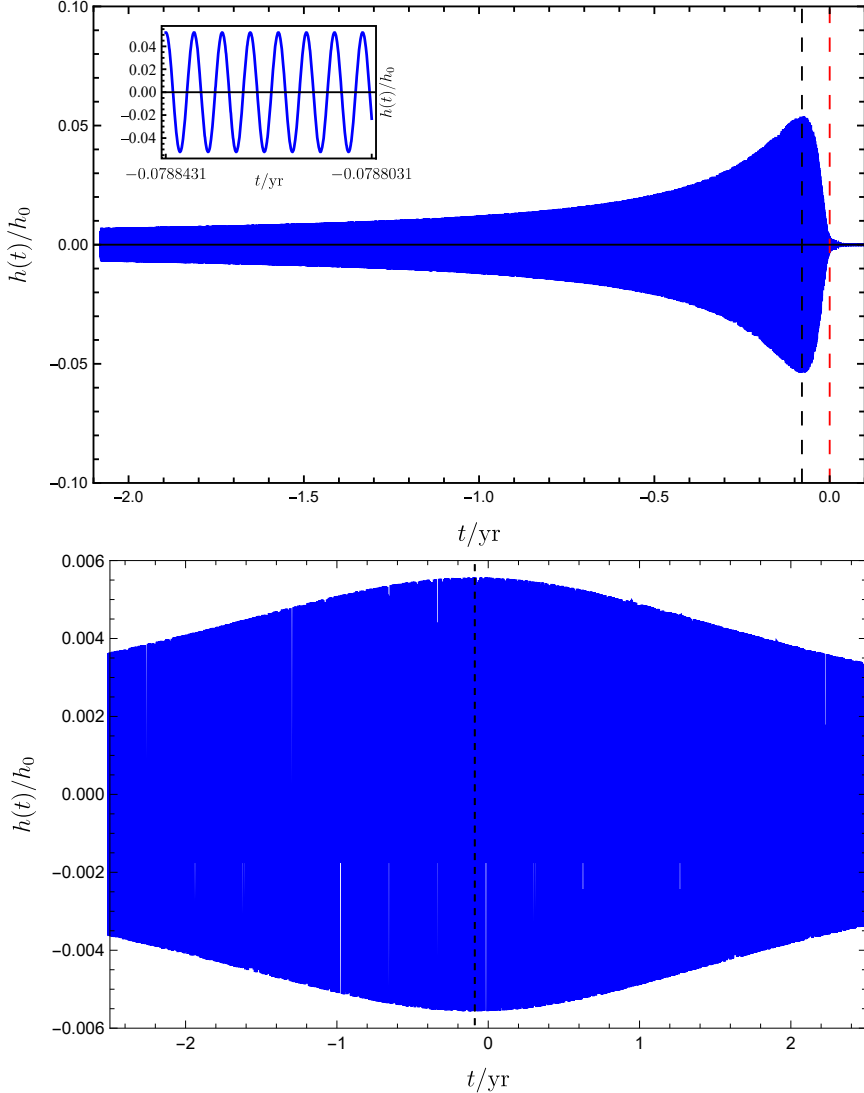


Figure 4: *top:* The plus polarization of the gravitational wave signal eq. (3.11) versus time. We have chosen $\alpha = 0.45$ and $q = 0.1$, and thus $z \approx 1.9$. The black hole mass is set to $M = 10^4 M_\odot$. The black dashed line is set at $t_{\text{max}} = -\frac{z|\Gamma|}{\gamma}$ and the red dashed line is at $t = 0$. The inset shows the oscillations around t_{max} . The normalization of the strain is $h_0 = 2.48 \times 10^{-22}$, assuming an event 20 Mpc away. *bottom:* Same as the top plot with $q = 10^{-3}$ and all other variables kept the same. The adiabaticity parameter is $z \approx 0.022$.

where ι is the angle between the line-of-sight of the observer and normal to the orbital plane of the system. The signal is therefore composed of a fast oscillating exponential term that contains information about the phase of the binary and an amplitude Q that contains the details of the transition. The amplitude of the strain is given by

$$h_0 = \frac{24M_c r_c^2 \Omega_0^2}{r} = 24 \frac{q_c M}{r} \frac{1}{\alpha^4} (M \Omega_0)^2, \quad (3.13)$$

where we defined $q_c(\alpha, \tilde{a}, m) \equiv \frac{M_c}{M}$ as the GA mass ratio and plugged in the expression for r_c in terms of α and M . The analysis regarding the mass of the GA is based on [39] and is laid out briefly in appendix C for the cases with one or more superradiant levels. The maximum value of q_c is close to 10%, when $\alpha = 0.24$, $m = 1$ and $\tilde{a} = 1$. We also stress that technically the mass of the black hole in eq. (3.13) should be calculated at the superradiant threshold, after the black hole has lost some of it due to superradiance. This fraction, however, is tiny and we shall ignore it in what follows. An estimate for this amplitude is

$$h_0 \approx 5.7 \times 10^{-22} \left(\frac{q_c}{0.1} \right) \left(\frac{M}{10^5 M_\odot} \right) \left(\frac{1 \text{Mpc}}{r} \right) \left(\frac{\alpha}{0.24} \right)^{10}. \quad (3.14)$$

The evolution of the strain versus the physical time is shown in fig. 4, for two specific choices of the parameters. The black dashed line is the time t_{max} when the amplitude Q is maximum, and thus that is when the strain reaches its maximum. The signal is oscillating because of the exponential factor $e^{-2i\Delta m\varphi(t)}$ and is otherwise modulated by the amplitude of Q .

In the case where $z \ll 1$, shown in the bottom plot of fig. 4, the exponential factor of eq. (2.34) does not play a big role in the evolution of the strain, which is predominantly regulated by $\frac{1}{i2\gamma t + |\Gamma|}$ in eq. (2.35). An estimate for the duration of the signal is given by

$$\Delta t_{211 \rightarrow 21-1} \sim 2 \frac{|\Gamma|}{\gamma} \approx 8.3 \text{years} \left(\frac{M}{10^4 M_\odot} \right) \left(\frac{10^{-3}}{q} \right) \left(\frac{0.45}{\alpha} \right)^{47/3}. \quad (3.15)$$

If $z \gtrsim 1$, as shown in the top plot of fig. 4, the strain has a tail at times $t \ll -\frac{z|\Gamma|}{\gamma}$, while it has significantly decayed at $t \sim 0$ due to the exponential in eq. (2.34). This causes it to be asymmetric around t_{max} . Since the starting time of the perturbation is roughly $t_I \sim -\frac{\Gamma}{\gamma}(1+2z)$, an estimate for the duration of the signal in this case is $\Delta t \sim 2\frac{|\Gamma|}{\gamma}(1+2z)$, which reduces to the previous result when $z \ll 1$.

The time-scale $\Delta t = 2\frac{|\Gamma|}{\gamma}(1+2z)$ is shown in fig. 5 for a wide range of mass ratios. As q and α decrease, the duration becomes longer and it may exceed the observational time-scale of an experiment. However, as long as $q \gtrsim 5 \times 10^{-3}$, the duration will be of order a few years or less for all the values of α we are considering.

Finally, we compute the radiated energy carried by this gravitational wave and compare that to the mass of the GA. Using the formula in [37], the radiated energy from gravitational waves is given by

$$\Delta E_{\text{rad}} = \frac{r^2}{16\pi} \int d^2\hat{\Omega} \int_{t_i}^{t_f} dt \left(\dot{h}_+^2 + \dot{h}_\times^2 \right). \quad (3.16)$$

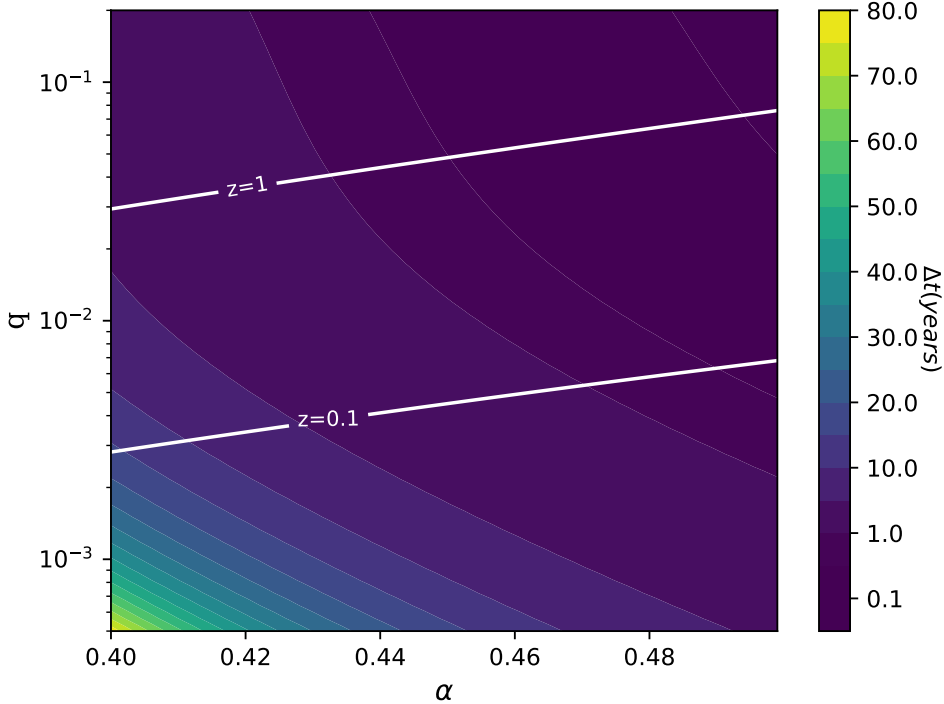


Figure 5: Duration of signal in days for $M = 10^4 M_\odot$. The white lines are contours of constant adiabaticity parameter z .

We will consider the limit where $z \ll 1$. Since we are interested in an order of magnitude estimate, we can argue that the angular integrals give only factors of $\mathcal{O}(1)$. For the time derivatives of the strains, using the previous arguments, we estimate them to be of order $\dot{h}_{+, \times} \sim \mathcal{O}(\Omega_0 h_{+, \times})$. Ignoring the fast oscillating terms in time and assuming that the integral is dominated at t_{\max} with a spread equal to Δt , the estimation gives

$$\frac{\Delta E_{\text{rad}}}{M_c} \sim r^2 h_0^2 \Omega_0^2 \frac{\Delta t}{M_c} |Q(t_{\max})|^2 \quad (3.17)$$

$$\approx 10^{-12} \left(\frac{q}{10^{-3}} \right) \left(\frac{\alpha}{0.45} \right)^{61/3} \left(\frac{1.81}{1 + 4\alpha^2} \right)^4, \quad (3.18)$$

where we approximated $|Q(t_{\max})|^2 \approx \frac{\eta^2}{|\Gamma|^2}$ and used eqs. (2.30) and (3.15). The radiated energy is therefore negligible compared to the mass of the GA.

3.2 The frequency spectrum

The frequency spectrum of the strain will be given by the Fourier transform:

$$\tilde{h}_{+, \times}(\omega) = \int_{t_i}^{t_f} dt h_{+, \times}(t) e^{i\omega t}, \quad (3.19)$$

where $t_i \sim -\frac{\Omega_0}{\gamma}$ and $t_f \sim \frac{\Omega_0}{\gamma}$, so that the linear approximation is valid within the domain of integration. Focusing on the plus polarization,

$$\tilde{h}_+(\omega) = h_0 \frac{1 + \cos^2 \iota}{2} \frac{e^{i\omega r}}{2} \int_{t_i}^{t_f} dt \left(e^{i(\omega t - 2\Delta m \varphi(t))} Q(t) + e^{i(\omega t + 2\Delta m \varphi(t))} Q^*(t) \right), \quad (3.20)$$

where we have renamed $t_{\text{re}} \rightarrow t$.

The stationary phase approximation can be used to evaluate the above integrals. The approximation is based on the fact that the integrals are dominated at the stationary points, that is, the points where the first derivative of the phase is zero. There are two stationary points in eq. (3.20), one for each term: $t_-(\omega) = -\frac{\omega + \omega_c}{2|\Delta m|\gamma}$ for the first integral and $t_+(\omega) = \frac{\omega - \omega_c}{2|\Delta m|\gamma}$ for the second integral, where we defined $\omega_c \equiv 2|\Delta m|\Omega_0 = 4\Omega_0$.

Evaluating the Q factors at the stationary points, Taylor expanding the phases around the stationary points up to order t^2 , and calculating the Gaussian integrals, we find

$$\tilde{h}_+(\omega) = \frac{\sqrt{\pi} h_0 (1 + \cos^2 \iota)}{4\sqrt{\gamma}|\Delta m|} \left(Q(t_-(\omega)) e^{i\Psi_-(\omega)} + Q^*(t_+(\omega)) e^{i\Psi_+(\omega)} \right), \quad (3.21)$$

with $\Psi_-(\omega) = \omega r - \frac{(\omega + \omega_c)^2}{4|\Delta m|\gamma} + \frac{\pi}{4}$ and $\Psi_+(\omega) = \omega r + \frac{(\omega - \omega_c)^2}{4|\Delta m|\gamma} - \frac{\pi}{4}$. From the discussion of the previous subsection, we can make use of the fact that the factor $|Q|$ peaks when $t_{\text{max}} = -\frac{z|\Gamma|}{\gamma}$.

For the first stationary point, this corresponds to frequency $\omega_c - 4z|\Gamma| = 4(\Omega_0 - z|\Gamma|)$ while for the second one to frequency $4z|\Gamma| - \omega_c = 4(z|\Gamma| - \Omega_0)$. From eqs. (2.17) and (2.28) and the analytical approximation for $|\Gamma|$, we have

$$\Omega_0 = \frac{6.88 \times 10^{-4}}{M} \left(\frac{\alpha}{0.45} \right)^7 \left(\frac{1.81}{1 + 4\alpha^2} \right), \quad (3.22)$$

$$z|\Gamma| \approx \frac{10^{-4}}{M} \left(\frac{q}{0.1} \right) \left(\frac{1.1}{1 + q} \right)^{5/3} \left(\frac{\alpha}{0.45} \right)^{19/3} \left(\frac{1.81}{1 + 4\alpha^2} \right)^{1/3}. \quad (3.23)$$

Therefore, for the parameters we are considering, the first frequency is always positive because $\Omega_0 - z|\Gamma| > 0$ and the second is always negative. Hence, keeping only the positive frequency in $\tilde{h}_+(\omega)$ in eq. (3.21) and using eq. (2.34) and eq. (2.35) to obtain Q , we get

$$\tilde{h}_+(f) = h_0 (1 + \cos^2 \iota) \sqrt{\pi} |\Delta m|^2 i e^{i\Psi_+(f)} \frac{\sqrt{z}}{|\Gamma| - i\pi(f - f_c)} e^{-\pi z} e^{-2z \tan^{-1}(\frac{\pi(f - f_c)}{|\Gamma|})}, \quad (3.24)$$

where we re-expressed the frequency in terms of $f = \frac{\omega}{2\pi}$. Similar results hold for $\tilde{h}_\times(f)$ that only differs by a phase of $\frac{\pi}{2}$. We therefore have an expression for the *peak frequency* of the signal

$$f_p = f_c - \frac{2z|\Gamma|}{\pi} = \frac{2}{\pi}(\Omega_0 - z|\Gamma|). \quad (3.25)$$

In fig. 6, we plot the dimensionless quantity $|\mathcal{I}_p(f)| = \sqrt{\gamma}|\Delta m| \frac{|\tilde{h}_+(f)|}{h_0}$, for the same parameters that we chose in fig. 4, versus the frequency f . In the bottom plot, we have chosen $z \ll 1$, in which case the signal is peaked at frequency $f_p \approx f_c = 4f_0 = \frac{2\Omega_0}{\pi}$ and is symmetric around that frequency. We also compare the numerical calculation with the

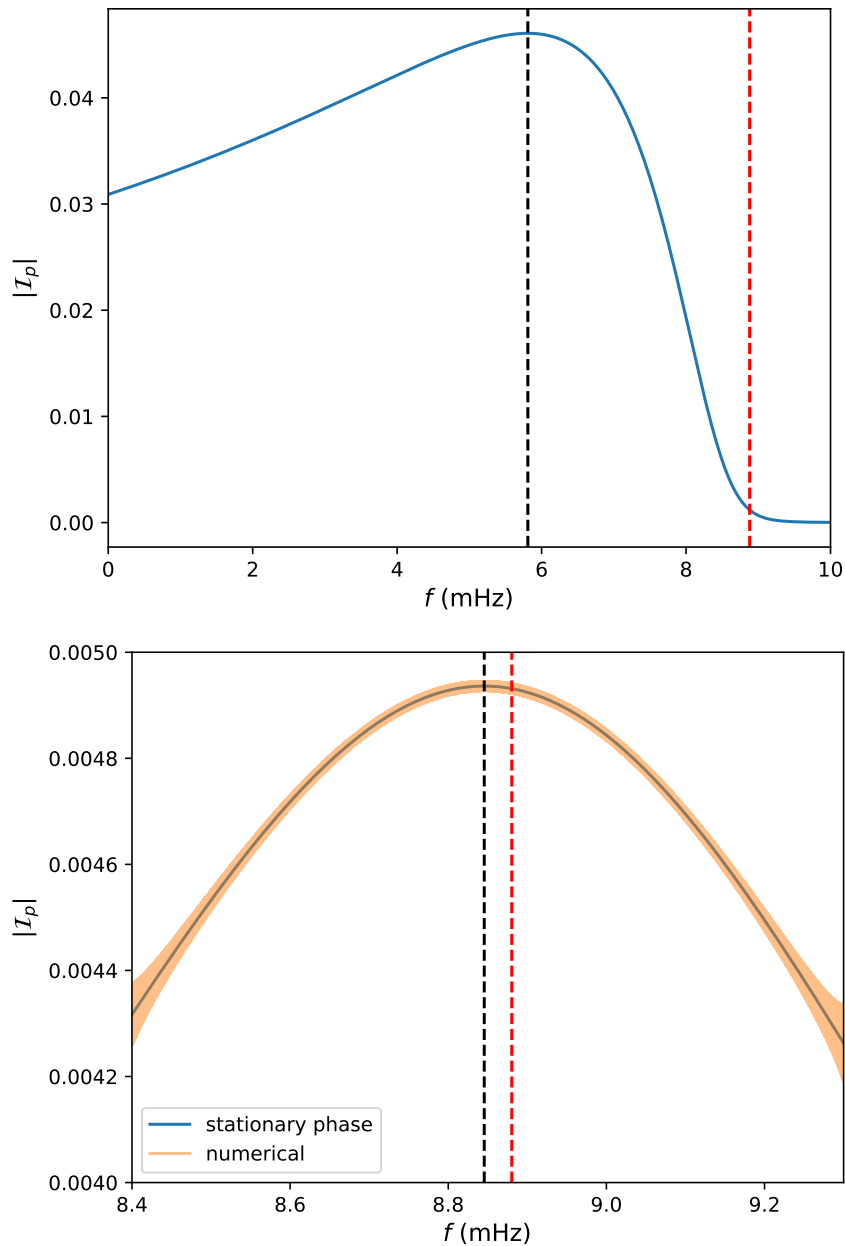


Figure 6: The factor $|\mathcal{I}_p| = \sqrt{\gamma|\Delta m|} \frac{|\tilde{h}_+(f)|}{h_0}$ versus frequency in mHz for the same parameters as in fig. 4. The black dashed line is the peak frequency $f_c - \frac{2z|\Gamma|}{\pi}$. The red dashed line in the top plot is $f_c = \frac{2\Omega_0}{\pi}$. In the bottom plot, we compare the stationary phase approximation and the numerical computation.

stationary phase approximation to demonstrate that the approximation is accurate, shown in the fig. 6 (bottom).

The *frequency spread* of the spectrum Δf can be further determined by eq. (3.24), in which the frequency spectrum is regulated by the factor $\frac{1}{|\Gamma| - i\pi(f-f_c)}$ when $z \ll 1$ and the contribution from the exponential function $e^{-2z \tan^{-1}(\pi(f-f_c)/|\Gamma|)}$ is negligible, indicating $\Delta f \approx \frac{4|\Gamma|}{\pi}$. We get explicitly:

$$\frac{\Delta f}{f_p} \approx 0.38 \left(\frac{\alpha}{0.45} \right)^3 \left(\frac{1 + 4\alpha^2}{1.81} \right), \quad (3.26)$$

so these types of transitions will be monochromatic.

In the top plot of fig. 6, we show \mathcal{I}_p for $z \sim \mathcal{O}(1)$. The signal now has decayed considerably at $f \sim f_c$, but it has a low-frequency tail that, based on our discussion for the duration of the signal, decays roughly at $f_{\min} \sim f_p - \frac{2|\Gamma|(2+3z)}{\pi}$. The frequency spread over the peak frequency is then:

$$\frac{\Delta f}{f_p} = \frac{f_c - f_{\min}}{f_c - 2z|\Gamma|/\pi} = \frac{2|\Gamma|(1+2z)}{\Omega_0 - z|\Gamma|}. \quad (3.27)$$

In the limit $z \ll 1$, we retrieve eq. (3.26). We plot this ratio in fig. 7 in the $\alpha - q$ plane. We observe that for close-to-equal mass binaries, the signal will not be monochromatic and its frequency will vary over a range of the order of f_p . This is to be expected, given the low-frequency tail in the top plot of fig. 6. When the mass ratio drops below $q \lesssim 0.04$, so that $z \lesssim 1$, the signal is essentially monochromatic.

We are now in the position to justify the use of the quadrupole approximation. In the case where $z \ll 1$, the wavelength of the signal is given by $\lambda \approx \frac{2\pi}{\omega_c} = \frac{\pi}{2\Omega_0}$. The size of the source is roughly the Bohr radius $r_c = \frac{M}{\alpha^2}$ and taking their ratio, we get

$$\frac{\lambda}{r_c} \approx 462 \left(\frac{0.45}{\alpha} \right)^5. \quad (3.28)$$

and therefore the approximation is expected to work very well. For larger values of z , the wavelength becomes larger, so the approximation becomes even more accurate.

3.3 The signal-to-noise ratio

The overall Fourier transformed signal is given by:

$$\tilde{h}(f) = F_+(\theta, \phi, \psi, f)\tilde{h}_+(\iota, f) + F_\times(\theta, \phi, \psi, f)\tilde{h}_\times(\iota, f), \quad (3.29)$$

where $F_{+, \times}(\theta, \phi, \psi, f)$ are the detector pattern functions that depend on the location in the sky (θ, ϕ) of the source and the polarization angle ψ of the signal. The power spectrum of the strain averaged over θ, ϕ, ψ and the inclination angle ι is given by

$$\langle S_h(f) \rangle = \langle \tilde{h}(f)\tilde{h}^*(f) \rangle = \langle F_+^2 \rangle \langle |\tilde{h}_+(\iota, f)|^2 \rangle + \langle F_\times^2 \rangle \langle |\tilde{h}_\times(\iota, f)|^2 \rangle = R(f) \left(\langle |\tilde{h}_+(\iota, f)|^2 \rangle + \langle |\tilde{h}_\times(\iota, f)|^2 \rangle \right), \quad (3.30)$$

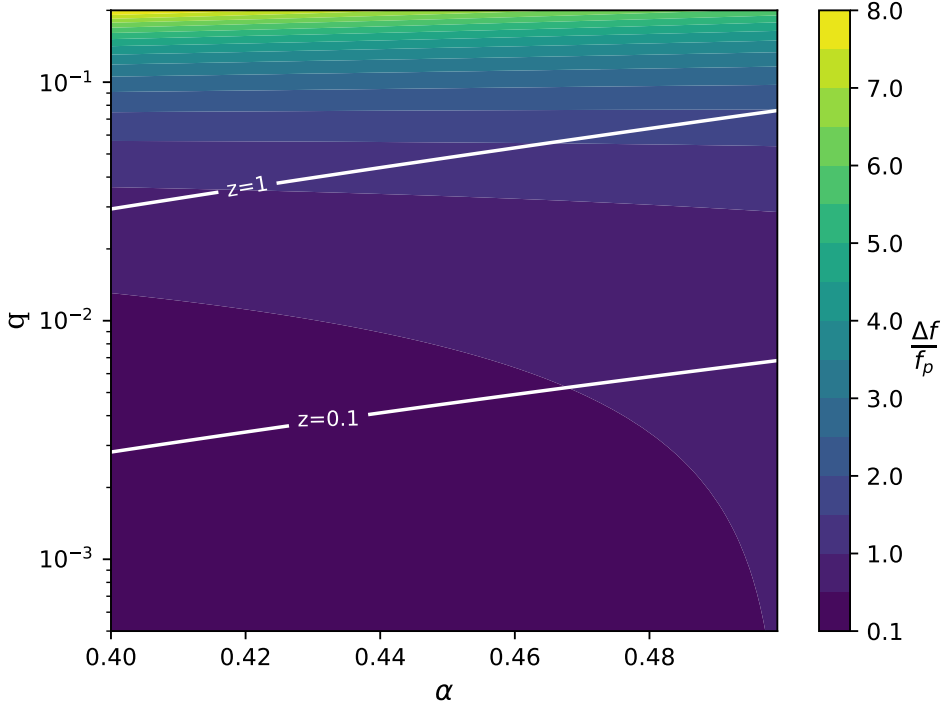


Figure 7: Contour plot of the ratio $\frac{\Delta f}{f_p}$ for the 211 transition. The white lines are contours of constant adiabaticity parameter z .

where $R(f) = \langle F_+^2 \rangle = \langle F_\times^2 \rangle$ is the interferometer response function and $\langle \dots \rangle$ represents the sky and polarization average. The averages over the inclination angle give

$$\langle |\tilde{h}_+|^2 \rangle = \frac{7\pi}{60} \left(\frac{h_0}{\sqrt{\gamma|\Delta m|}} \right)^2 |Q(t_+(f))|^2, \quad (3.31)$$

$$\langle |\tilde{h}_\times|^2 \rangle = \frac{\pi}{12} \left(\frac{h_0}{\sqrt{\gamma|\Delta m|}} \right)^2 |Q(t_+(f))|^2, \quad (3.32)$$

where we used eq. (3.21) and kept only the contribution from positive frequencies. The angle averaged power spectrum is given by

$$\langle S_h \rangle = \frac{\pi}{5} R(f) \left(\frac{h_0}{\sqrt{\gamma|\Delta m|}} \right)^2 |Q(t_+(f))|^2. \quad (3.33)$$

Finally, the square of the signal-to-noise ratio is

$$\text{SNR}^2 = 4 \int_{f_{\min}}^{f_{\max}} df \frac{\langle S_h \rangle}{R(f)S_n(f)} = \frac{4\pi}{5} \frac{h_0^2}{\gamma|\Delta m|} \int_{f_{\min}}^{f_{\max}} df \frac{|Q(t_+(f))|^2}{S_n(f)}, \quad (3.34)$$

where $S_n(f)$ is the noise power spectrum of LISA [40] and we set $f_{\max} = 1\text{Hz}$, $f_{\min} = 10^{-5}\text{Hz}$. The factor $Q(t_+(f))$ is given in eq. (3.10) in terms of the coefficients d_1 and d_2

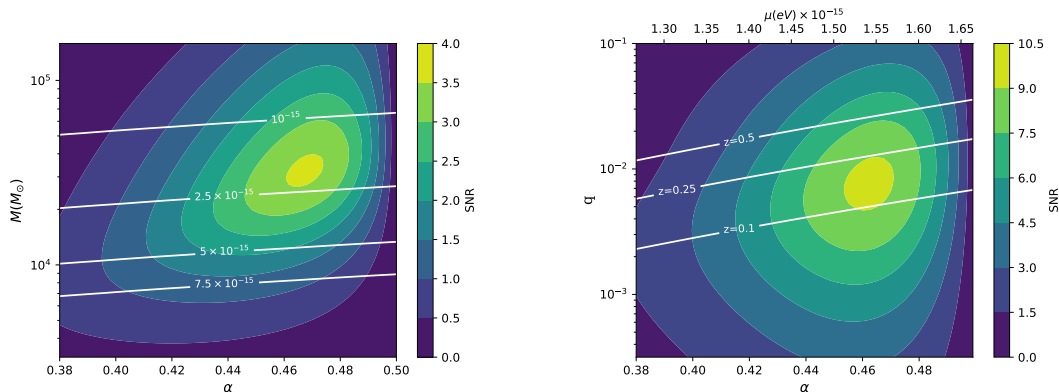


Figure 8: *left:* Contours of the SNR values for different black hole masses and parameters α for the $211 \rightarrow 21-1$ transition. The mass ratio is set to $q = 0.1$ and the distance is 20Mpc. The white lines are boson masses in eV. *right:* Contours of the SNR values for different mass ratios and parameters α . The black hole mass is set to $M = 4 \times 10^4 M_\odot$. The upper x axis shows the corresponding boson masses in eV and white contours are values of the adiabaticity z .

and we can readily use eq. (2.34) and eq. (2.33), since in the parameter space of interests, it is always the case that $\eta \ll |\Gamma|$.

4 Implications

4.1 LISA binary systems

We will start this section by considering stellar mass black holes in binary systems that reside in the Mikly Way. In [41], using the FIRE simulation data, it was predicted that around a million binary black holes are present in the Milky Way with a mean mass of $28M_\odot$, while approximately only 20 of them would be detected by LISA. Those that would be detected have frequency close to 0.3mHz. From eq. (2.19), we see that this corresponds to $\alpha \approx 0.12$ for a gravitational wave emitted during the 211 hyperfine transition. Using the expression of strain h_0 in eq. (3.13), we can obtain an estimate for the amplitude:

$$h_{0,\text{MW}} = 2.4 \times 10^{-25} \left(\frac{M}{30M_\odot} \right)^{17/7} \left(\frac{1\text{kpc}}{r} \right) \left(\frac{f_0}{0.3\text{mHz}} \right)^{10/7}. \quad (4.1)$$

This amplitude is too small to produce a sizable SNR at this frequency. This leads us to consider Intermediate Mass Black Holes (IMBH). These have masses in the range $10^2 - 10^5 M_\odot$ and are thought to form through successive mergers in dense stellar environments [42]. A wide range of mass ratios is also possible $q \sim 1 - 10^{-5}$, depending on the specific IMBH and its environment. In the left plot of fig. 8, using eq. (3.34), we show the SNR values for a range of black hole masses and α values in binaries with $q = 0.1$ for the $211 \rightarrow 21-1$, having set the distance to $r = 20\text{Mpc}$ for all events. The white lines are contours of the boson masses measured in eV. For black hole masses $M \in [3, 4] \times 10^4 M_\odot$ and $\alpha \in$

[0.46, 0.475], values that correspond to boson masses in the range $\mu \in [1.5, 2.1] \times 10^{-15} \text{eV}$, the SNR is maximized. It depends on α and M in a complicated way through z , $|\Gamma|$ and γ , but we do expect it to be maximized due to the variation in frequency as we vary these two parameters (see eq. (2.19) and eq. (3.25)). These specific values give us a peak frequency in the range $f_p \in [1.7, 2.5] \text{mHz}$, close to the frequencies where LISA will be at its best sensitivity [40].

In the right plot of fig. 8, we fixed the black hole mass to be $M = 4 \times 10^4 M_\odot$ and varied the mass ratio. Interestingly, the SNR can now increase compared to the previous case. It is maximized when $q \in [5 \times 10^{-3}, 1.5 \times 10^{-2}]$ and $\alpha \in [0.45, 0.47]$. As it can be seen from the contours of the adiabaticity parameter, this maximum occurs when $0.1 < z < 0.25$. Calculating the ratio $|Q(t_+(f))|^2/S_n(f)$ at the central frequency $f_p = 2(\Omega_0 - z|\Gamma|)/\pi$ as a function of z , we have

$$\frac{|Q(t_+(f_p))|^2}{S_n(f_p)} \propto \frac{z}{1 + 4z^2} \frac{e^{-2\pi z + 4z \tan^{-1}(2z)}}{S_n(\frac{2}{\pi}(\Omega_0 - z|\Gamma|))}, \quad (4.2)$$

where we used eqs. (2.34) and (2.35). For α in the range of interest, we find that this quantity is indeed maximized at $z \approx 0.18$, which corresponds to mass ratio $q \approx 8.2 \times 10^{-3}$ (see eq. (2.28)). These results are indeed reflected in fig. 8.

4.2 Breaking degeneracies by spectral information

The gravitational wave signal produced by a GA transition (GAT) triggered by the tidal perturbation from a companion has distinct features in gravitational wave spectra for different types of transitions. Compared with the continuous gravitational wave signal discussed in [6] due to the spontaneous transition between boson states, the signal studied in this work contains richer information about the binary system and thus one has more handles to disentangle the signal from the background that mimics the signal. In this subsection, we demonstrate an example of combining the binary system and spectral information of the GAT signal to break the degeneracies of the model parameters. By using the peak frequency f_p , the width Δf , and the amplitude $A(f_p)$, one could try to understand what kind of information we obtain for the GA and the binary system. The discussion below uses the same assumptions throughout the paper: the black hole spin is saturated, i.e., $\tilde{a} = \tilde{a}_{\text{crit}}(m_i) = \frac{4m_i\alpha}{m_i^2 + 4\alpha^2}$ such that the boson mass is fixed to be the maximum value that can be produced by superradiance $\mu = m_i\Omega_H$, where m_i is the azimuthal quantum number of the initial boson state, and the companion is moving in a co-rotating, quasicircular, and equatorial orbit.

As we have seen, the peak frequency of the gravitational wave spectrum is given in eq. (3.25), which depends on the black hole mass M , fine-structure constant α , the quantum numbers of the initial state $|nlm_i\rangle$ and the mass ratio q :

$$f_p = f_p(\mu, n, l, m_i; M, q), \quad (4.3)$$

where we implicitly set the black hole mass M and the mass ratio q as known input parameters which can be obtained by the observed inspiral gravitational wave spectrum or other

types of measurements such as the X-ray measurement for X-ray binaries. Thus one can relate the dependence of the boson mass to the fine-structure constant $\mu = \alpha/M$.

The width of the GAT gravitational wave frequency spectrum was determined in equation eq. (3.27) and it depends on the same set of parameters, that is

$$\Delta f = \Delta f(\mu, n, l, m_i; M, q). \quad (4.4)$$

Finally, the amplitude of the signal was determined in eqs. (3.13), (3.24) and (3.33), denoted as $A(f_p) = \sqrt{\langle S_h(f_p) \rangle}$ and its dependence on the model parameters is given by

$$A(f_p) = A(f_p)(\mu, q_c, n, l, m_i; M, q, r), \quad (4.5)$$

where r is the distance from the source to the gravitational wave detector, which can be inferred by the inspiral gravitational wave measurement, and q_c is the cloud mass ratio compared to the central black hole mass. The expression for q_c is given in appendix C and it depends on the black hole's mass, the initial spin, the boson mass and the third quantum number m_i :

$$q_c = q_c(\mu, m_i, \tilde{a}_i; M). \quad (4.6)$$

Hence, the parameters that determine the amplitude of the GAT are:

$$A(f_p) = A(f_p)(\mu, n, l, m_i, \tilde{a}_i; M, q, r). \quad (4.7)$$

An observed GAT signal can measure these three quantities, f_p , Δf , and $A(f_p)$. Assuming, as we discussed, that M , q and r are known from the observation of the gravitational waves of the inspiral, the spectrum depends on the five unknowns $\{\mu, \tilde{a}_i, n, l, m\}$, so there are not enough data to determine them. One would have to assume that the signal originated from a particular transition, the $211 \rightarrow 21-1$ for example, and then the initial spin of the black hole and the boson mass could be inferred.

4.3 Dependence on mass ratio q : phase shift and Doppler shift

Let us imagine two cases, $q \ll 1$ and $q \gtrsim 1$. In the first case, the position of the rotating BH remains nearly unchanged relative to the center of mass. However, in the second case, the rotating BH orbits around the center of mass of the system. The q dependence manifests as a phase shift in the waveform and a frequency shift caused by the Doppler effect. These two effects introduce distinguishable features in the gravitational waves from the transitions, relative to those from the inspiral binary motion.

The phase shift is due to varying location of the rotating black hole, and so it is proportional to the distance between the rotating black hole and the center of mass. The distance for the circular motion is

$$R_* = (GM)^{1/3} \frac{q}{(1+q)^{2/3}} \Omega^{-2/3}. \quad (4.8)$$

Thus, the phase shift at the resonance of the transition $\Omega(t) = \Omega_0$ would be on the order of

$$\begin{aligned} \frac{R_*}{\lambda} &\simeq \frac{|\Delta m|}{\pi} (M\Omega_0)^{1/3} \frac{q}{(1+q)^{2/3}} \\ &\simeq 3.5 \times 10^{-2} \left(\frac{q}{1}\right) \left(\frac{2}{1+q}\right)^{2/3} \left(\frac{\alpha}{0.45}\right)^{7/3} \left(\frac{1.81}{1+4\alpha^2}\right)^{1/3}, \end{aligned} \quad (4.9)$$

where $\lambda = \frac{2\pi}{\omega_c}$ is the wavelength of the GAT gravitational wave at resonance.

We can also see that the Doppler effect is of the same order of magnitude since the Doppler shift in frequency is proportional to v_{rel}/c ,

$$\frac{v_{\text{rel}}}{c} = \frac{R_*\Omega_0}{c} \simeq \frac{\pi}{|\Delta m|} \frac{R_*}{\lambda}. \quad (4.10)$$

These two effects are next-to-leading-order contributions, suppressed by a factor of $R_*/\lambda \sim v_{\text{rel}}/c$. Therefore, the leading-order contribution to the gravitational wave strain must be sufficiently large to compensate for this suppression: $h(t) \simeq h_{\text{inspiral}}^{(0)}(t) + h_{\text{transition}}^{(0)}(t) + \delta h_{\text{phase}}(t) + \delta h_{\text{Doppler}}(t)$, where $\delta h_i/h_{\text{transition}}^{(0)} \simeq \mathcal{O}(R_*/\lambda)$. In frequency space, although each strain component generally appears at a different frequency, they are typically on the order of $f_{\text{GW}} \simeq \mathcal{O}(\Omega/(2\pi))$. In particular, δh_i should exhibit periodic behavior due to the periodic orbital motion. In terms of noise, these effects can correspond to time jitter noise, which can be seen in the LISA phasemeter [43, 44].

5 Conclusion

In this paper, we have developed a formalism to calculate the gravitational wave signal produced by the atomic transition of GA in a binary system. In the perturbative regime where the companion's orbital distance is much larger than the size of the GA, the dominant multipole moment of the tidal field from the companion is the quadrupole moment $l_* = 2$, which gravitationally mixes two GA states and thus triggers the transition. We find that the energy density of the GA is non-axisymmetric due to the interference of the two states during the transition and therefore it develops a time-dependent quadrupole moment, resulting in gravitational wave emission.

The two-state transition of a tidally perturbed GA is modeled by the Landau-Zener system, in which we included the decay of the bosons in the final state back to the black hole to capture the intricate dynamics of the system. Under the assumption of quasicircular and equatorial orbit, and linearized orbital frequency, the analytical formulae of the gravitational wave strain waveform and frequency spectrum are derived. We validate the parameter region of (α, q) for the linearized orbital frequency approximation for the $211 \rightarrow 21-1$ hyperfine and $322 \rightarrow 300$ fine transition. For phenomenological interests, we restrict our attention to the former for mass ratios $q \lesssim 0.2$.

The gravitational wave signal from the resonant transition of tidally perturbed GA exhibits distinguishable features compared to other existing astrophysical gravitational wave signals. The generic feature of the strain waveform is that it can be considered a continuous signal with amplitude modulated by the LZ transition, with its peak amplitude at the resonance for intermediate and extreme mass ratio inspirals. The duration of the signal is determined by the adiabaticity parameter z , the decay rate of the final state Γ , and the change rate of the orbital frequency due to inspiral gravitational wave emission γ . It is of order $\mathcal{O}(\text{yr})$ for $q \gtrsim 5 \times 10^{-3}$, while it increases as q decreases. We stress that the analytical waveform of the signal can serve as the template used by the match-filtering technique for future gravitational wave searches.

The gravitational wave frequency spectrum is derived analytically using the stationary phase approximation. The analytical result is in good agreement with the numerical result. The frequency spectrum is characterized by three important quantities: peak frequency f_p , frequency spread Δf , and amplitude $A(f_p)$. The decay of the final state detunes the peak frequency of the signal from $f_p = 4f_0$, where $f_0 = \Omega_0/(2\pi)$ is the orbital frequency at resonance, to $f_p = 4f_0 - 2z|\Gamma|/\pi$. Depending on the parameters and the particular transition, this signal may or may not be monochromatic, i.e., whether $\Delta f/f_p \ll 1$ or not. The signal is typically monochromatic when $q \lesssim 0.04$, while it becomes a broad-band signal for larger mass ratio q .

In terms of the detection of the signal, we focus on the IMBH binaries at the LISA's frequency band. We apply our formalism to calculate the SNR for such systems, varying the central black hole mass M , the mass ratio q , and the fine-structure constant α . We found that, for close to equal mass binaries, the most promising events will occur from black holes with masses $M \in [3, 4] \times 10^4 M_\odot$ and boson mass $\mu \in [1.5, 2.1] \times 10^{-15}$ eV. By fixing the black hole mass to $M = 4 \times 10^4 M_\odot$ and varying q , we found that the SNR more than doubled compared to the case of equal mass binaries, while it is maximized for $q \in [5 \times 10^{-3}, 10^{-2}]$.

Furthermore, we explore the implications of the potential detection of the signal. We study how to combine the observation of both inspiral and GAT gravitational wave signals to disentangle the degeneracies of the model parameters. By fixing the quantum numbers n, l, m of the initial state, the measurement of the peak frequency, frequency spread, and amplitude can determine the boson mass μ and the initial black hole spin \tilde{a}_i . We stress that this type of analysis requires knowledge of the black hole masses and distance from Earth, which can be obtained from an observation of the inspiral gravitational waves of the binary. In addition, we estimate the phase shift of the gravitational wave signal due to the motion of the primary black hole around the center of mass of the binary system to be $\mathcal{O}(0.01)$.

To streamline the analysis, several assumptions are made. We now discuss potential follow-up studies in the future to improve it:

- The simplifying assumption of quasicircular and equatorial orbits, for example, needs to be refined. It has been found that if we relax these assumptions, transitions can occur at a variety of frequencies [21, 45]. The detectability of the GAT signal in this case is something worth examining.
- Taking into account the back-reaction of the transition to the orbit is another important topic. This is manifested through the conservation of angular momentum for the entire system. The gravitational waves that we have found will contribute to the total torque of the system, possibly leading to non-trivial dynamics of the orbit. This interplay between the back-reaction of the transition and the back-reaction of the emitted gravitational waves might lead to unexpected and interesting behavior for the binary's orbit.
- In terms of environmental effects, since the black holes that would produce the largest SNR are of intermediate mass that are typically found in dense globular clusters,

incorporating the perturbations to the cloud from nearby stars and quantifying their influence on the cloud’s evolution, perhaps in the spirit of [46], would be an interesting direction.

- Finally, we have glossed over the fact that our signal is relevant for relatively large values of α . The non-relativistic approximation is expected to deviate from the real solution when $\alpha \gtrsim 0.2$. A relativistic computation that takes into account this deviation would be an important addition in this line of research and we hope to follow up on this in the future.

Acknowledgments

We are grateful to Hyeonseok Seong for pointing out the phase shift of the waveform, the calculations in appendix B and the many interesting discussions. We are also thankful to Astrid Lamberts for providing the FIRE simulation dataset. Additionally, we want to thank Jeff Dror, John Stout, Rachel Houtz, Wei Xue, Yue Zhao and Joseph Fichera for their insightful and useful discussions. F.Y. and A.K. are supported in part by the U.S. Department of Energy under grant DE-SC0022148 at the University of Florida. AK is also supported by the Onassis Foundation - Scholarship ID: F ZS 031-1/2022-2023.

A Gravitational atom basics

A.1 Tidal field of the companion

We present in this appendix some of the formulae we used for the tidal field of the companion and the Hamiltonian for the two state system. The tidal field is given as a sum over multipoles:

$$V_*(t, \vec{r}) = -q\alpha \sum_{l_*=2} \sum_{|m_*| \leq l_*} \mathcal{E}_{l_*, m_*}(\iota_*, \varphi_*) Y_{l_*, m_*}(\theta, \phi) \left(\frac{r^{l_*}}{R_*^{l_*+1}} \Theta(R_* - r) + \frac{R_*^{l_*}}{r^{l_*+1}} \Theta(r - R_*) \right), \quad (\text{A.1})$$

where R_* is the distance of the companion from the primary black hole, $\mathcal{E}_{l_*, m_*}(\iota_*, \varphi_*)$ is the tidal moment (see Appendix A of [20] for details), ι_* is the inclination of the orbital plane relative to the GA’s, φ_* is the true anomaly and is related to the frequency of the binary via $\dot{\varphi}_*(t) = \pm\Omega(t)$. We have also defined $q = \frac{M_*}{M}$ as the mass ratio.

Assuming that the quadrupole dominates, the mixing between two states $|\psi_i\rangle$ and $|\psi_f\rangle$ is given by

$$\langle \psi_f | V_*(t, \vec{r}) | \psi_i \rangle = \mathcal{E}_{2, m_*}(\iota_*, \varphi_*) I_A \left(\frac{qM\Omega}{\alpha^3(1+q)} I_{\text{in}} + \frac{\alpha^7 q(1+q)^{2/3}}{(M\Omega)^{7/3}} I_{\text{out}} \right), \quad (\text{A.2})$$

where the inner radial, outer radial, and angular overlaps of the initial and final wavefunction mediated by the quadrupole moment of the tidal field are:

$$I_{\text{in}} = \int_0^{R_*/r_c} d\bar{r} \bar{r}^4 \bar{R}_i(r_c \bar{r}) \bar{R}_f(r_c \bar{r}), \quad (\text{A.3})$$

$$I_{\text{out}} = \int_{R_*/r_c}^{\infty} d\bar{r} \bar{r}^{-1} \bar{R}_i(r_c \bar{r}) \bar{R}_f(r_c \bar{r}), \quad (\text{A.4})$$

$$I_A = \int d\Omega Y_{l_*, m_*}(\theta, \varphi) Y_i(\theta, \varphi) Y_f^*(\theta, \varphi), \quad (\text{A.5})$$

with new dimensionless quantities $\bar{r} = \frac{r}{r_c}$ and $\bar{R}(r_c \bar{r}) = R(r) r_c^{3/2}$. The selection rules eq. (2.9) are derived from the last angular integral. Taking $l_* = 0$, the amplitude of the mixing normalized by the orbital frequency is:

$$\frac{\eta}{\Omega} = \left| \sqrt{\frac{3\pi}{10}} I_A \left(\frac{qM\Omega}{\alpha^3(1+q)} I_{\text{in}} + \frac{\alpha^7 q(1+q)^{2/3}}{(M\Omega)^{7/3}} I_{\text{out}} \right) \right|. \quad (\text{A.6})$$

and the matrix element is given in eq. (2.12).

A.2 Dressed frame Hamiltonian

In the dressed co-rotating frame, the Hamiltonian is given by:

$$\bar{\mathcal{H}} = \begin{pmatrix} -\frac{\Delta m}{2} \left(\frac{\Delta \omega_R}{\Delta m} \mp \Omega(t) \right) & \eta \\ \eta & \frac{\Delta m}{2} \left(\frac{\Delta \omega_R}{\Delta m} \mp \Omega(t) \right) - i|\Gamma| \end{pmatrix}. \quad (\text{A.7})$$

Choosing $\Omega_0 = \pm \frac{\Delta \omega_R}{\Delta m}$ and using eq. (2.13), we obtain the Hamiltonian of the Landau-Zener system (for a co-rotating orbit),

$$\bar{\mathcal{H}} = \begin{pmatrix} \frac{\Delta m}{2} \gamma t & \eta \\ \eta & -\frac{\Delta m}{2} \gamma t - i|\Gamma| \end{pmatrix}. \quad (\text{A.8})$$

The second order differential equations for $d_1(t)$ and $d_2(t)$ are

$$d_i''(\tau) + d_i(\tau) \left(\frac{\tau^2}{4} - \frac{i}{2} + z \right) = 0, \quad (\text{A.9})$$

$$d_f''(\tau) + d_f(\tau) \left(\frac{\tau^2}{4} + \frac{i}{2} + z \right) = 0, \quad (\text{A.10})$$

where we have defined $\tau = \sqrt{|\Delta m|} \gamma t$ and set $\Gamma = 0$. The prime denotes the derivative with respect to τ . The solutions to these equations are given in eqs. (2.23) and (2.24) and are plotted in fig. 1.

B Axially asymmetric density from interference

As shown in Sec. 3.1, the interference term between states is a key to generate quadrupole moment through non-trivial dependence of the energy density on ϕ . Since the rotating BH is axisymmetric, one might expect that so is the cloud.

A state ψ is introduced in the ansatz of the real scalar field Φ such that

$$\Phi(t, \mathbf{x}) = \frac{1}{\sqrt{2\mu}} (\psi(t, \mathbf{x})e^{-i\mu t} + \text{h.c.}). \quad (\text{B.1})$$

The energy density of Φ is approximately

$$\rho_\Phi \simeq \frac{1}{2}\dot{\Phi}^2 + \frac{1}{2}(\nabla\Phi)^2 + \frac{1}{2}\mu^2\Phi^2 + V_{\text{grav}}(r, \theta). \quad (\text{B.2})$$

If we consider a mixed state,

$$\psi(t, \mathbf{x}) = c_1(t)\psi_1(t, \mathbf{x}) + c_2(t)\psi_2(t, \mathbf{x}), \quad (\text{B.3})$$

the scalar field Φ would be

$$\Phi = \sqrt{\frac{2}{\mu}} |c_1| |\psi_1| \cos(m_1\phi - \omega_1 t + \delta_1) + (1 \leftrightarrow 2), \quad (\text{B.4})$$

where $\delta_i(t)$ is the phase of $c_i(t)$, and $\psi_i = |\psi_i| e^{im_i\phi} e^{-i(\omega_i - \mu)t}$ is used.

$$\begin{aligned} \frac{1}{2}\mu^2\Phi^2 &= \mu|c_1|^2|\psi_1|^2\cos^2(m_1\phi - \omega_1 t + \delta_1) + \mu|c_2|^2|\psi_2|^2\cos^2(m_2\phi - \omega_2 t + \delta_2) \\ &\quad + 2\mu|c_1||c_2||\psi_1||\psi_2|\cos(m_1\phi - \omega_1 t + \delta_1)\cos(m_2\phi - \omega_2 t + \delta_2). \end{aligned} \quad (\text{B.5})$$

On the other hand,

$$\dot{\Phi} \simeq \sqrt{\frac{2}{\mu}} |c_1| |\psi_1| (\omega_1 - \dot{\delta}_1) \sin(m_1\phi - \omega_1 t + \delta_1) + (1 \leftrightarrow 2), \quad (\text{B.6})$$

thus the kinetic term becomes

$$\begin{aligned} \frac{1}{2}\dot{\Phi}^2 &\simeq \frac{(\omega_1 - \dot{\delta}_1)^2}{\mu} |c_1|^2 |\psi_1|^2 \sin^2(m_1\phi - \omega_1 t + \delta_1) + \frac{(\omega_2 - \dot{\delta}_2)^2}{\mu} |c_2|^2 |\psi_2|^2 \sin^2(m_2\phi - \omega_2 t + \delta_2) \\ &\quad + \frac{2(\omega_1 - \dot{\delta}_1)(\omega_2 - \dot{\delta}_2)}{\mu} |c_1||c_2||\psi_1||\psi_2| \sin(m_1\phi - \omega_1 t + \delta_1) \sin(m_2\phi - \omega_2 t + \delta_2), \end{aligned} \quad (\text{B.7})$$

$$\simeq \mu|c_1|^2|\psi_1|^2\sin^2(m_1\phi - \omega_1 t + \delta_1) + \mu|c_2|^2|\psi_2|^2\sin^2(m_2\phi - \omega_2 t + \delta_2)$$

$$+ 2\mu|c_1||c_2||\psi_1||\psi_2|\sin(m_1\phi - \omega_1 t + \delta_1)\sin(m_2\phi - \omega_2 t + \delta_2). \quad (\text{B.8})$$

We keep the leading order terms in the limit where $\omega_i \simeq \mu \gg \Omega$, $\omega_i - \mu$, γ/η . The spatial derivative term in the energy density is also suppressed by $1/r_c = \alpha^2/M = \alpha\mu$ with respect to the time derivative resulting in μ . Therefore, the energy density of Φ is approximately

$$\rho_\Phi \simeq \frac{1}{2}\dot{\Phi}^2 + \frac{1}{2}\mu^2\Phi^2 + V_{\text{grav}}(r, \theta), \quad (\text{B.9})$$

$$\simeq \mu|c_1|^2|\psi_1|^2 + \mu|c_2|^2|\psi_2|^2 + 2\mu|c_1||c_2||\psi_1||\psi_2|\cos(\Delta m\phi - \Delta\omega t + \Delta\delta) + V_{\text{grav}}. \quad (\text{B.10})$$

By taking an angular derivative along ϕ ,

$$\frac{d\rho_\Phi}{d\phi} \simeq -2\Delta m\mu|c_1||c_2||\psi_1||\psi_2|\sin(\Delta m\phi - \Delta\omega t + \Delta\delta), \quad (\text{B.11})$$

which means the energy density distribution is not axisymmetric, and hence the GA in a mixed state can emit gravitational waves. In short, the coherent wave nature makes an asymmetric energy density distribution out of axisymmetric energy distributions for each state through the constructive or destructive interference between states.

C The mass of the GA

In this appendix, we calculate the mass that is stored in the GA when the black hole has reached the superradiant threshold $\mu = m\Omega_H$. The dimensionless spin and the mass at the threshold are given by [39]:

$$M' = \frac{m^2}{8\mu\alpha} \frac{1 - \sqrt{1 - \left(\frac{4\alpha}{m}\left(1 - \frac{\alpha\tilde{a}}{m}\right)\right)^2}}{1 - \frac{\alpha\tilde{a}}{m}}, \quad (\text{C.1})$$

$$\tilde{a}' = \frac{4\alpha}{m} \left(1 - \frac{\alpha\tilde{a}}{m}\right). \quad (\text{C.2})$$

The quantities with prime are calculated at the superradiant threshold while the unprimed are the initial ones. The parameter α is understood as $\alpha = \mu M$. The factor q_c is then given by

$$q_c = \frac{M_c}{M'} = \frac{M - M'}{M'} = \frac{8\alpha^2 \left(1 - \frac{\alpha\tilde{a}}{m}\right)}{m^2 \left(1 - \sqrt{1 - \left(\frac{4\alpha}{m}\left(1 - \frac{\alpha\tilde{a}}{m}\right)\right)^2}\right)} - 1. \quad (\text{C.3})$$

This is for the case where only one mode is present. Following the analysis of [39], when we include a higher energy mode, the effect of superradiance into that mode can be modeled as a form of accretion. When this accretion starts, the black hole loses spin, rendering the original mode decaying. The second mode grows, while the GA loses mass to the black hole, which moves up along the superradiant threshold in the Regge plane. Eventually, the first mode decays completely and the black hole follows a new trajectory, which stops at the superradiant threshold of the second mode. The mass fraction of the GA in the second mode will be given by

$$q_c = \frac{M'}{M''} - 1, \quad (\text{C.4})$$

where M'' is the mass of the black hole at the second superradiant threshold, which is found by eq. (C.1) with the replacement $M' \rightarrow M''$ and $m \rightarrow m'$. We therefore get for the mass fraction

$$q_c = \left(\frac{m}{m'}\right)^2 \frac{1 - \frac{\alpha\tilde{a}}{m'} \frac{1 - \sqrt{1 - \left(\frac{4\alpha}{m}\left(1 - \frac{\alpha\tilde{a}}{m}\right)\right)^2}}{1 - \frac{\alpha\tilde{a}}{m}}}{1 - \frac{\alpha\tilde{a}}{m} \frac{1 - \sqrt{1 - \left(\frac{4\alpha}{m'}\left(1 - \frac{\alpha\tilde{a}}{m'}\right)\right)^2}}{1 - \frac{\alpha\tilde{a}}{m}}} - 1. \quad (\text{C.5})$$

References

- [1] R. Brito, V. Cardoso and P. Pani, *Superradiance: New Frontiers in Black Hole Physics*, *Lect. Notes Phys.* **906** (2015) pp.1 [1501.06570].
- [2] D.J.E. Marsh, *Axion Cosmology*, *Phys. Rept.* **643** (2016) 1 [1510.07633].
- [3] M. Cirelli, A. Strumia and J. Zupan, *Dark Matter*, **2406.01705**.
- [4] S.L. Detweiler, *KLEIN-GORDON EQUATION AND ROTATING BLACK HOLES*, *Phys. Rev. D* **22** (1980) 2323.

- [5] D. Baumann, H.S. Chia, J. Stout and L. ter Haar, *The Spectra of Gravitational Atoms*, *JCAP* **12** (2019) 006 [[1908.10370](#)].
- [6] A. Arvanitaki and S. Dubovsky, *Exploring the String Axiverse with Precision Black Hole Physics*, *Phys. Rev. D* **83** (2011) 044026 [[1004.3558](#)].
- [7] A. Arvanitaki, M. Baryakhtar and X. Huang, *Discovering the QCD Axion with Black Holes and Gravitational Waves*, *Phys. Rev. D* **91** (2015) 084011 [[1411.2263](#)].
- [8] C. Ünal, F. Pacucci and A. Loeb, *Properties of ultralight bosons from heavy quasar spins via superradiance*, *JCAP* **05** (2021) 007 [[2012.12790](#)].
- [9] S.J. Witte and A. Mummery, *Stepping Up Superradiance Constraints on Axions*, [2412.03655](#).
- [10] S. Hoof, D.J.E. Marsh, J. Sisk-Reynés, J.H. Matthews and C. Reynolds, *Getting More Out of Black Hole Superradiance: a Statistically Rigorous Approach to Ultralight Boson Constraints*, [2406.10337](#).
- [11] V.M. Mehta, M. Demirtas, C. Long, D.J.E. Marsh, L. McAllister and M.J. Stott, *Superradiance Exclusions in the Landscape of Type IIB String Theory*, [2011.08693](#).
- [12] M. Baryakhtar, M. Galanis, R. Lasenby and O. Simon, *Black hole superradiance of self-interacting scalar fields*, *Phys. Rev. D* **103** (2021) 095019 [[2011.11646](#)].
- [13] V.M. Mehta, M. Demirtas, C. Long, D.J.E. Marsh, L. McAllister and M.J. Stott, *Superradiance in string theory*, *JCAP* **07** (2021) 033 [[2103.06812](#)].
- [14] R. Brito, S. Ghosh, E. Barausse, E. Berti, V. Cardoso, I. Dvorkin et al., *Gravitational wave searches for ultralight bosons with LIGO and LISA*, *Phys. Rev. D* **96** (2017) 064050 [[1706.06311](#)].
- [15] J. Yang and F.P. Huang, *Gravitational waves from axions annihilation through quantum field theory*, *Physical Review D* **108** (2023) .
- [16] H. Omiya, T. Takahashi, T. Tanaka and H. Yoshino, *Deci-Hz gravitational waves from the self-interacting axion cloud around a rotating stellar mass black hole*, *Phys. Rev. D* **110** (2024) 044002 [[2404.16265](#)].
- [17] S. Collaviti, L. Sun, M. Galanis and M. Baryakhtar, *Observational prospects of self-interacting scalar superradiance with next-generation gravitational-wave detectors*, *Class. Quant. Grav.* **42** (2025) 025006 [[2407.04304](#)].
- [18] D. Baumann, H.S. Chia and R.A. Porto, *Probing Ultralight Bosons with Binary Black Holes*, *Phys. Rev. D* **99** (2019) 044001 [[1804.03208](#)].
- [19] G.M. Tomaselli, T.F.M. Spieksma and G. Bertone, *Legacy of Boson Clouds on Black Hole Binaries*, *Phys. Rev. Lett.* **133** (2024) 121402 [[2407.12908](#)].
- [20] D. Baumann, H.S. Chia, R.A. Porto and J. Stout, *Gravitational Collider Physics*, *Phys. Rev. D* **101** (2020) 083019 [[1912.04932](#)].
- [21] G.M. Tomaselli, T.F.M. Spieksma and G. Bertone, *Resonant history of gravitational atoms in black hole binaries*, *Phys. Rev. D* **110** (2024) 064048 [[2403.03147](#)].
- [22] T. Takahashi, H. Omiya and T. Tanaka, *Axion cloud evaporation during inspiral of black hole binaries: The effects of backreaction and radiation*, *PTEP* **2022** (2022) 043E01 [[2112.05774](#)].
- [23] D. Baumann, G. Bertone, J. Stout and G.M. Tomaselli, *Ionization of gravitational atoms*, *Phys. Rev. D* **105** (2022) 115036 [[2112.14777](#)].

- [24] D. Baumann, G. Bertone, J. Stout and G.M. Tomaselli, *Sharp Signals of Boson Clouds in Black Hole Binary Inspirals*, *Phys. Rev. Lett.* **128** (2022) 221102 [2206.01212].
- [25] T. Takahashi, H. Omiya and T. Tanaka, *Self-interacting axion clouds around rotating black holes in binary systems*, *Phys. Rev. D* **110** (2024) 104038 [2408.08349].
- [26] A. Guo, J. Zhang and H. Yang, *Superradiant clouds may be relevant for close compact object binaries*, *Phys. Rev. D* **110** (2024) 023022 [2401.15003].
- [27] T. Takahashi, H. Omiya and T. Tanaka, *Evolution of binary systems accompanying axion clouds in extreme mass ratio inspirals*, *Phys. Rev. D* **107** (2023) 103020 [2301.13213].
- [28] M. Bošković, M. Koschnitzke and R.A. Porto, *Signatures of Ultralight Bosons in the Orbital Eccentricity of Binary Black Holes*, *Phys. Rev. Lett.* **133** (2024) 121401 [2403.02415].
- [29] X. Tong, Y. Wang and H.-Y. Zhu, *Termination of superradiance from a binary companion*, *Phys. Rev. D* **106** (2022) 043002 [2205.10527].
- [30] S.M. Carroll, *Spacetime and Geometry: An Introduction to General Relativity*, Cambridge University Press (7, 2019), 10.1017/9781108770385.
- [31] L.D. Landau, *A theory of energy transfer. 2.*, *Phys. Z. Sowjetunion* **2** (1932) .
- [32] C. Zener, *Nonadiabatic crossing of energy levels*, *Proc. Roy. Soc. Lond. A* **137** (1932) 696.
- [33] X. Tong, Y. Wang and H.-Y. Zhu, *Gravitational Collider Physics via Pulsar–Black Hole Binaries II: Fine and Hyperfine Structures Are Favored*, *Astrophys. J.* **924** (2022) 99 [2106.13484].
- [34] N.M. Temme, “NIST Digital Library of Mathematical Functions.”
- [35] V.M. Akulin and W.P. Schleich, *Landau-zener transition to a decaying level*, *Phys. Rev. A* **46** (1992) 4110.
- [36] N.V. Vitanov and S. Stenholm, *Pulsed excitation of a transition to a decaying level*, *Phys. Rev. A* **55** (1997) 2982.
- [37] M. Maggiore, *Gravitational Waves. Vol. 1: Theory and Experiments*, Oxford University Press (2007), 10.1093/acprof:oso/9780198570745.001.0001.
- [38] R. Shankar, *Principles of quantum mechanics*, Plenum, New York, NY (1980).
- [39] L. Hui, Y.T.A. Law, L. Santoni, G. Sun, G.M. Tomaselli and E. Trincherini, *Black hole superradiance with dark matter accretion*, *Phys. Rev. D* **107** (2023) 104018 [2208.06408].
- [40] T. Robson, N.J. Cornish and C. Liu, *The construction and use of LISA sensitivity curves*, *Class. Quant. Grav.* **36** (2019) 105011 [1803.01944].
- [41] A. Lamberts, S. Blunt, T.B. Littenberg, S. Garrison-Kimmel, T. Kupfer and R.E. Sanderson, *Predicting the LISA white dwarf binary population in the Milky Way with cosmological simulations*, *Mon. Not. Roy. Astron. Soc.* **490** (2019) 5888 [1907.00014].
- [42] A. Askar, V.F. Baldassare and M. Mezcua, *Intermediate-Mass Black Holes in Star Clusters and Dwarf Galaxies*, 11, 2023 [2311.12118].
- [43] LISA collaboration, *LISA Definition Study Report*, 2402.07571.
- [44] D. Shaddock, B. Ware, P.G. Halverson, R.E. Spero and W. Klipstein, *Overview of the LISA phasemeter*, *AIP Conf. Proc.* **873** (2006) 654.

- [45] E. Berti, R. Brito, C.F.B. Macedo, G. Raposo and J.L. Rosa, *Ultralight boson cloud depletion in binary systems*, *Phys. Rev. D* **99** (2019) 104039 [[1904.03131](#)].
- [46] V. Dandoy, T. Schwetz and E. Todarello, *A self-consistent wave description of axion miniclusters and their survival in the galaxy*, *JCAP* **09** (2022) 081 [[2206.04619](#)].